Northumbria
University
NEWCASTLE

Formation of gradient microstructure and mechanical properties of hot-pressed W-20wt.%Cu composites after sliding friction severe deformation

L.L. Dong[a], M. Ahangarkani[b], W. Zhang[a], B. Zhang [c, a], W.G. Chen[c], Y.Q. Fu [d], Y.S. Zhang[a*]

[a] Advanced Materials Research Central, Northwest Institute for Nonferrous Metal Research, Xi'an 710016, China

[b] Department of Materials, Malek Ashtar University of Technology, Tehran, Iran

[c] School of Materials Science and Engineering, Xi'an University of Technology, Xi'an 710048, China

[d] Faculty of Engineering and Environment, Northumbria University, Newcastle upon Tyne, NE1 8ST, UK.

Abstract:

W-based alloys are currently considered promising candidates for high heat flux components in future fusion reactors. In this paper, hot pressed W-20wt.%Cu composites were treated at room temperature using a sliding friction severe deformation (SFD) process, with a moving speed of 0.2 m/s and an applied load of 500 N. Microstructural evolution of composites after the SFD treatment was evaluated and compared with that of the untreated composites. Results showed that there was a gradient structure generated and an obvious refinement in tungsten particles size in

* Corresponding authors: Professor Y.S. Zhang
E-mail addresses: y.sh.zhang@163.com, y.s.zhang@c-nin.com (Y.S. Zhang)

the surface layer after the SFD process. The average particle size of tungsten in the SFD treated composites was 2.60 μm, whereas it was 4.5 μm for tungsten in the untreated composites. Fracture surfaces of the composites indicated that the SFD treatment destroyed the W skeleton and changed fracture mode from predominant inter-granular one to trans-granular one due to the decrease in contact area of W-W inter-particles. Yield strength and ultimate tensile strength of composites after the SFD treatment were 308 MPa and 553 MPa, respectively. The treated composites exhibited micro-hardness values with an average reading of about 308 HV. Analysis of the facture microstructures clearly suggested that the tungsten particles in the treated composites are consisted of dislocations and boundaries as well as dislocation tangles. The electrical conductivity of the composites was decreased from 33 IACS% to 28.5 IACS% after the SFD treatment, mainly due to loss or squeezing of copper into the inner surface.

Keywords: W-Cu composites; Sliding friction treatment; Microstructure; Mechanical properties

1. Introduction

Tungsten-copper (W-Cu), a typical composite consisting of W particles embedded inside Cu matrix, has received much attention for the manufacture of electrical contact parts, heat sinks in high-power microelectronic devices, arcing-resistant electrodes and deviator plates for fusion reactors in armour materials,

owing to their excellent properties including low coefficient of thermal expansion, high hardness, high melting point of W and excellent thermal and electrical conductivity of Cu [1-3]. However, the W-Cu composites have potential drawbacks such as poor toughness, which restrict their wide applications in many stringent service conditions in industry applications [4-5]. This is mainly because W and Cu have no mutual solubility over the whole range of composition range in W-Cu composites at various temperatures, therefore, it is critical to explore new synthesis technologies to improve their mechanical properties and thus expand their wide-range applications.

Over the past decades, a considerable amount of work has been focused on the preparation and enhancement of physical properties of W-Cu composites [6-10]. However, few studies have been devoted to the detailed microstructural evolution and mechanical properties of W-Cu composites, especially after surface treatments such as severe plastic deformation (SPD). A number of researchers have investigated the deformation behavior and properties of Al alloys, Mg alloys, Ti alloys and pure metals (Ta and Cu) processed by the SPD processes [11-16], including equal channel angular extrusion/pressing (ECAE/ECAP), high pressure torsion (HPT), surface mechanical attrition treatment , ultrasonic hot peening, ball burnishing, as well as sliding friction treatment deformation (SFD). Among these approaches, SFD is a surface strengthening technology with a great potential for industrial applications. It can be used to fabricate a nanocrystalline (nc) or ultrafine grain layer on the surface of treated bulk metals. Along with other surface treatment technologies, SFD is now

widely used in preparation of many types of gradient nanostructured materials. For example, Zhang reported an nc-structured layer with grains of 7 nm on the surface of pure Ta using the SFD [17]. However, the grain coarsening was found in nc-Cu due to the high stress, high strain and large amplitude occurred in the SFD process of Cu [17]. Deng et al. reported that the micro-hardness values of the nanoscale lamellae and fine deformed grains of pure Cu were ~1.85 GPa and 1.2~1.5 GPa, respectively, after rapid platen friction sliding deformation [18]. Sabirov et al investigated the effect of SPD process on coarse-grained W-Cu composites. They found that the W-Cu composites were thermally stable dual-phase composites, where the W exhibited a strong temperature dependent yield strength and was much more brittle than Cu and HPT, thus causing a strong refinement of W particles [19]. Also, W-Cu composites with good electrical conductivity (46.8% IACS) and high micro-hardness (450 HV) were achieved by multiple treatments at high temperature and high pressure deformation processes [20]. Recently, Dong et al succeeded in fabrication of W-Cu composites using an ECAP, and achieved an effective refinement of W grains after the ECAP process [21]. However, so far, there is no report on SFD processes of WCu composites, and it would be of great scientific interesting to study gradient microstructure formation and mechanical property enhancement of WCu composites after the SFD treatment.

In this paper, SFD technology was proposed to conduct on W-Cu composites. Microstructure evolution and properties of the W-Cu composites after SFD treatment was investigated. The deformation mechanism of the SFD-treated (hereafter we use

the abbreviation of SFDed) W-Cu composites was explored and discussed. The study of this work will expand wide range applications of the W-Cu composites through microstructural changes and improvement in the mechanical properties of the composites.

2. Experimental

2.1 Raw materials

The materials under investigation in this work were W80-Cu20 composites (i.e. 80wt.% W and 20wt.% Cu) fabricated using hot pressing sintering. The W powder (~6μm, ＞99.99%wt.%) and Cu powder (~48μm, ＞99.99%wt.%) were blended in a V-type mixing machine for 8h, followed by hot pressing sintering. The detailed processing parameters of hot pressing sintering are listed in Table 1. Samples with a size of 200×100×5 (mm×mm×mm) were obtained using a wire-cutting machine as shown in Fig. 1(a). Fig. 1(b) shows a scanning electron microscope (SEM) cross-section image of the polished W80-Cu20 composites. The dark and bright regions are Cu and W phases, respectively.

Table 1 Processing parameters of fabrication of W80-Cu20 composites by hot pressing sintering.

Fig. 1 (a) Photo showing the sample dimensions; (b) SEM image of cross-section of polished W80-Cu20 composites.

2.2 SFD treatment

The experiments were conducted on a specially designed set-up with a ball-on-disc contact configuration as shown in Fig. 2(a). A schematic illustration of the SFD process is presented in Figs. 2(b) ~ (e).

(1) Firstly, a spherical WC-Co ball with a diameter of 10 mm was sliding under a normal load against a metal sheet along the X direction from left to right at a velocity of v_1 and a preset amplitude of d_1 (Fig. 1(b)). In this step, a wide furrow parallel to the sliding direction was induced in the wake of the sliding event.

(2) Secondly, the metal plate was shifted in the Y direction for a distance of d_2 at a velocity of v_2 followed by sliding along the X direction from right to left with a distance of d_1 (Fig. 1(c)). When the ball slided back to the left, a shallow plow mark was generated because of the small value of d_2 compared with the width of the primary furrow (Fig. 1(d)).

(3) Repeated friction was conducted, and as a consequence, the sample surface showed roughened surfaces and a plastically deformed layer on the surface of W-Cu composites (Fig. 1(e)).

In order to effectively refine the grains in the surface layer, the SFD process was repeated 20 times with the same processing parameters as follows: load F (500 N), moving speed v_1 (0.2 m/s), v_2 (0.005 m/s) and feeding step distance d (0.1mm).

Fig. 2 (a) The designed set-up for SFD process; (b) ~ (e) an illustration of the step-by-step SFD processes.

2.3 Materials characterization

The microstructure and particle size of untreated and SFDed W80-Cu20 composites

were characterized using a JEOL-JSM6460 SEM equipped with energy dispersive spectroscopy (EDS), as well as a transmission electron microscope (TEM) observations were carried out using a FEI Tecani F30. For the TEM sample preparation, about 0.5 mm thin foil of the treated surface layer was obtained via using wire-cutting machine, mechanically ground to a thickness of 40~50 μm used metallographic sand paper, and then a thickness of 15~20 μm was performed by dimpling grinder. The final thinning was carried out using a Gatan PIPS 691 ion milling system with a time of 12 h and argon ions were used in the ion etching with the accelerating voltage in the range of 2.5-5 keV and with the incident angle in the range of 4~10 ° at room temperature. About two hundred particles within the same size scope of SEM images are randomly selected to statistically analyze the average size of W particles using Nano Measurer software. X-ray diffraction (XRD) using a Dmax-2500 diffractometer with Cu K_α (λ=0.15418nm) radiation was performed on the SFDed composites to determine the crystalline phases. The diffraction profiles were measured in the 2θ angle range of 10-90^o with a scan step of 0.02^o. Textures are prospected by X-ray diffraction on a Xpert Pro MRD with a Cu K_a radiation. The measurement was done along cross section direction of the samples. The Jtex V.2.20 software was employed for plotting pole and inverse pole figures and analyzing the texture data. Fig. 3 shows the observing location of the texture testing.

The densities of the specimen were measured by the Archimedes displacement method. The electrical conductivity was determined using an Eddy Current Conductivity Meter (D60K). The micro-hardness of the surface was measured using a

Vicker's hardness tester (MVS-1000JMT2) under a load of 50 g and a dwell time of 10 s. The average of 10 indents was used to ensure acquisition of a reasonable value of microhardness. The Instron 5848 Microtester was used to test the tensile properties and fracture behavior of W80-Cu20 composites at room temperature with a strain rate of 1×10^{-3} s^{-1}. Three samples were tested for the tensile strength tests to acquire the average value. The tensile fracture surfaces of the W80-Cu20 composites were investigated using the SEM to determine the failure mechanism.

3. Results and discussion

Fig. 4 shows the microstructures of the cross-sectioned surface of untreated and SFDed W80-Cu20 composites. In Fig. 4(a), the Cu phase is uniformly distributed throughout the composites, in which the average particle size of W is about 4.5 μm, which can be observed from the statistical particle size distribution of W as shown in Fig. 4(c). After the SFD treatment, the W particles exhibit a significant reduction in particle size with an average value of 2.60 μm, as well as severe and inhomogeneous deformation (Fig. 4(d) and Fig. 4(b)). It can be concluded that W particles have been refined after the SFD process. Similar phenomenon has been observed in Mg alloys by Huo et al [22], who reported that an average grain size of 70 nm on the topmost surface was obtained after 100 cycle repeated sliding friction treatment.

On the other hand, EDS mapping results shown in Fig. 4(e) and 4(f) demonstrate the inhomogeneous deformation of W skeleton during the SFD. As indicated, region A in Fig. 4(f) contains lower Cu content and refined W particles due to significant

deformation. Inversely, region B in Fig. 4(f) contains higher Cu content and exhibits similar microstructural features to those in the untreated composites as shown in Fig. 3(e).

Fig. 4 The cross-section SEM images of (a) W80-Cu20 composites and (b) SFDed composites after 20 cycle sliding treatment, (c) and (d) statistical distribution of the W grain size of W particles in Fig. (a) and (b), respectively, (e) and (f) elemental mapping analysis results from W80-Cu20 composites and SFDed composites after 20 cycle sliding treatment, respectively.

SEM micrographs of the longitudinal cross-section of W80-Cu20 composites before and after SFD process are illustrated in Fig. 5. A plastic deformed surface layer with a thickness of about 50 μm was created after SFD process, as observed in Fig. 5(b). By comparing Figs. 5(a) and Fig. 5(b), the W particles are obviously refined under the repeated frictional sliding. Figs. 5(c) and (d) are higher magnification SEM images of the SFDed sample showing the microstructure at the edge and in the center area of the sample, respectively. In Fig. 5(c), the W particles are elongated in parallel to sliding moving direction.

According to the EDS results of the wear debris (shown in the top right corner in Fig. 5(c)), the Cu content in Fig. 5(c) is lower than that in Fig. 5(a) owing to the loss or squeezing of Cu from the composites during the SFD treatment. On the other hand, the W particles obviously exhibit a fragmentation phenomenon and are slightly elongated as shown in Fig. 5(d). Also, EDS mapping in Figs. 5(e) and 5(f) illustrates that the SFD process results in the development of a gradient surface microstructure

due to the application of sliding load. As can be seen from these figures, the Cu phase at the near-surface area was reduced due to the loss or squeezing of Cu during SFD treatment. However, it is gradually increased with an increase in the distance from the surface, and ultimately reached to the same composition as that in the untreated composites. Formation of a gradient microstructure generated in pure copper by platen friction sliding deformation has also been reported by Deng et al [23] and Figueroa et al [24].

The evolution of gradient microstructure of W-Cu composite during SFD treatment can be described by two main steps: (1) refinement of W particles and rotation towards the sliding direction, together with decrease of spacings between W particles in deformed skeleton; and (2) loss or squeezing of Cu at near-surface areas during SFD process. As a result, although such fine scale structures with lower Cu content can be developed at the top surface, the center of the deformed layer does not show apparent microstructural changes.

Fig. 5 The longitudinal cross-sectioned SEM images of W80-Cu20 composites: (a) original W80Cu20 composites; (b) SFDed composite after 20 cycles; (c) in the edge area; (d) in the center area. (e) and (f) elemental mapping analysis results from W80-Cu20 composites and SFDed composites after 20 cycle sliding treatments, respectively.

XRD patterns of the untreated and SFDed W80-Cu20 composites are shown in Fig. 6, which reveals that no phase transformation occurred in the W80-Cu20 composites after SFD process. By Comparing Fig. 6(a) and Fig. 6(b), a broadening of

the W phase peaks was observed, which could be induced by grain refinement and lattice strain accumulation.

Fig. 6 XRD patterns of the W80-Cu20 composites; (a) original composites and (b) SFDed composites after 20 cycle treatments.

In order study the texture changed before and after SFD treatment, the XRD was used to characterize the texture of the surface of W particles and the results are shown in Fig. 7. The origional W-Cu composites have a low texture strength, as observed in Fig. 7(a). However, in Fig. 7(b), the SFD treament on the surface of the composites have changed the intensity of texture. The stable texture components was further informed, including Brass type texture {110} <112>, Copper type texture{211} <111> and rotating cubic texture {200} <011>. The changes in basal texture intensities witness the increased strength of composite.

Fig. 7 Pole figure (110), (200) and (211) of orgional W80-Cu20 composites (a) and SFDed W80-Cu20 composites (b) taken along cross section direction of the samples.

The measured relative density, electrical conductivity and micro-hardness of the W80-Cu20 composites before and after SFD treatment are presented in Table 2. The electrical conductivity of the sample is decreased from 33 IACS% to 28.5 IACS% after SFD treatment, because of the lower Cu content in the SFDed composites as well as the refinement of W particle. However, the relative density of the SFDed composites has a value of 98.5% which is higher than that of untreated composites due to the elongation and fragmentation of W particle. Also, a significant increase in the hardness of W80-Cu20 composites was obtained after SFD treatment. Its micro-hardness is 308 HV, which is higher than that of the untreated composites (Table 2).

Table 2 The electrical conductivity, relative density and micro-hardness of the W80-Cu20 composites in the work.

Fig. 8 shows TEM images of e microstructure and deformation behavior of W80-Cu20 composites after the SFD process. Figs. 8(a) ~ (c) indicate that the grains of the composites which are composed of W phases embedded inside a Cu matrix. The Cu phase is a typical FCC crystal structure (Fig. 8(b)) and W phase is a typical BCC crystal structure (Fig. 8(c)), based on the SAED patterns. Fig. 8(d) presents a TEM image of the W phase in the SFDed composite and the inset is the corresponding SADE pattern. It can be observed that dislocations and grain boundaries are clearly existed in the deformed W particles, and dislocation tangles are also found in Fig. 8(d). It should be noted that there are some deformation twins marked by the yellow circles observed in the deformed composites, as determined by the EDS (In Fig. 8(f)). From the high-resolution image shown in Figs. 8(e), the lattice spacing was measured, and the lattice value is 0.356 nm, which is corresponding to W (110) (cf JCPDS file No. 33-13870) (as shown in the inset of the Fig. 8(e)). It is well known that the plastic deformation of metallic materials is a competition between dislocation movement and deformation twinning processes [25].

Fig. 8 (a) TEM image of W80-Cu20 composites, (b) electron diffraction pattern of position 1 in Fig. 8(a); (c) electron diffraction pattern of position 2 in Fig. 8(a); (d) TEM image of deformed W80-Cu20 composites; (e) high magnification of marked 3 zone in Fig. 8(d) and inset shows high-magnification images of twinning, (f) EDS of marked position 3 zone in Fig. 8(d).

The tensile stress-strain curves of the W80-Cu20 composites before and after the SFD treatment are plotted in Fig. 9(a). The effect of sliding friction on the tensile strength and elongation of the composites are shown in Fig. 9(b). It can be seen that both the stress-strain curves of untreated and treated composites show a similar trend (i.e. elastic deformation, followed by plastic deformation, before the final fracture of the samples). However, the SFDed W80-Cu20 composites exhibit much higher yield (YS) and ultimate tensile strength (UTS) than those of the untreated composites. The YS and UTS of the SFDed W80-Cu20 composites are 308.74 MPa and 553.60 MPa, respectively, which are about 16.93% and 6.13% higher than those of the untreated composites. The higher tensile strength of SFDed composite is mainly attributed to the fine W particles and higher density of the composites. The effects of particle size of W on mechanical properties have also been observed by Gong et al [26], who reported that the finer W grains are beneficial to obtain deformation strengthening because of the higher amount of grain boundaries in the fine-grained alloy than those in the alloys with larger grains. The reduced grain size should be the most important factor in strengthening of the composites in this work. Theoretically, the larger grain size often leads to the poor mechanical properties at room temperature [27]. In addition, the higher mechanical properties of the SFDed composites are attributed to the reduction of Cu phase due to the squeezing of the Cu phase from the surface into the sub-layer. The elongation to failure of the SFDed W80-Cu20 composites is 2.0%, which is of 65.3% lower compared to 5.77% of untreated composites.

Fig. 9 (a) Tensile stress-strain curves and (b) summaries of the data of the W80-Cu20 composites and 20 cycles SFDed composites, respectively.

The fracture surfaces of W80-Cu20 composites before and after SFD treatment are shown in Fig. 10. The W particle is lighter in color while the Cu phase is darker in color in these pictures. The smooth and nearly round areas represent the W-W inter-granular fracture mode of W at its grain boundaries. As illustrated in Fig. 10(a), W particles in untreated composites mainly demonstrated inter-granular brittle fracture. The fracture surfaces of W particles show many large dimples, and hence, the failure of composites with high content of W occurs by separation of W/W to produce cleaved W grains (with river-bank like feature as indicated in Fig. 10(a)) after strain hardening of the Cu phase and fracture of the matrix [28]. The W-W interface in W-Cu composites is the places where the fracture occurring, mainly due to existence of some small impurity phase particles, such as oxides and brittle compounds at the grain boundaries.

Figs. 10(b) and (c) are SEM micrographs of SFDed composites close to the surface and in the center area of the sample, respectively. As can be seen, the centerregion of the SFDed sample (Fig. 10(b)) has a similar fracture surface with those of the untreated composite (Fig. 10(a)), while there is a change in the fracture mode in the edge areas after SFD treatment (Fig. 10(c)). It confirms the development of gradient microstructure due to severe plastic deformation after the SFD treatment.

As illustrated in Fig. 10(c), the W skeleton has been completely deformed. For this reason, unlike the fracture surfaces in Fig. 10(a) and Fig. 10(b), W-W contiguity

is decreased completely. W-W contiguity is a microstructural feature in W-Cu composite and is related to number of bonds between adjacent tungsten particles. In other word, W-W contiguity is directly proportional to total W-W interfaces. In addition, the particle size of W decreases which leads to the reduction in uniformity of the composite structure. It can be concluded that the SFD treatment leads to a decrease in the W-W contiguity, a significant reduction in particle size, and a gradual change in microstructure in the surface area of the SFDed W80-Cu20 composites.

In summary, the sliding friction deformation results in two apparent changes in microstructure based on the analysis of fracture surfaces of the composites:

(I) At regions near to the surface (region A in Fig. 4(f)), tungsten particles are completely separated from each other due to destroying of the tungsten skeleton (Fig. 10(c)). This leads to the diminish of W-W interfaces and significant reduction in tungsten particle size after treatment. The fracture surface shows trans-granular fracture mode in SEM images as shown in Fig. 10(c).

(II) At regions beneath the exposure surface (region B in Fig. 4(f)), inter-granular fracture takes place due to applied load. However, the load applied to this region is less than the external applied load. This reduced load results in the lower level of deformation. Therefore, it can only separate tungsten particles from each other, but will not be able to break up the tungsten particles and reduce their sizes. The fracture surface shows trans-granular mode as shown in Fig. 10(b), which has a structure similar to that of the original material (Fig. 10(a)).

Fig. 10 SEM images near the surface area of the composites (a) the original W80-Cu20

composites, (b) center area of the SFDed composites; and (c) edge area of the SFDed composite.

The schematic illustration of the SFD treatment of W80-Cu20 composites is presented in Fig. 11. Fig. 11(a) shows the microstructure of the untreated W80-Cu20 composites. The gray regions are the W skeleton composed of W particles, the black lines are W-W grain-boundaries, and the orange regions are Cu phases filled inside the W skeleton. Firstly, the W-W boundaries start to crack, followed by the collapse of W skeleton into fragmented skeletons under the repeated sliding friction treatment. However, in Fig. 11(b), the Cu exhibits a significant plastic deformation owing to its low strength and high ductility, while the W particles exhibit very slight deformation because the W-W boundaries are the weak points and hence intergranular separation of W grains easily occurs [29]. With further sliding deformation, more W-W boundaries are separated, and more fragmented skeletons collapse into smaller W particles (in Fig. 11(c)). These smaller W particles are further elongated. The Cu phase exhibits a much more severe deformation, wrapping the W particles and accommodating the plastic deformation of the W80-Cu20 composites. The Cu content in the SFDed W80-Cu20 composites (as shown in Fig. 11(c)) is lower than that in the untreated composites (as shown in Fig. 11(a)). This is due to the low bond strength between the mechanically mixed W particles and Cu. As a result, Cu could be reduced from the surface of the SFDed W80-Cu20 composites during the SFD process.

Fig. 11 Schematic illustrations of the deformation process of the W80-Cu20 composites during SFD process: (a) the original microstructure of the W80-Cu20 composites; (b) the collapse of the

W skeleton; and (c) further deformation of the W particles.

4. Conclusions

In this study, sliding friction treatment method was applied on the W80-Cu20 composites. Cross-section microstructure, fracture mode and tensile/electrical properties of the SFDed W-Cu composites were investigated. The following conclusions can be drawn from the present work:

(1) W particles of composites were significantly refined during sliding friction treatment. After sliding friction, the W particles with an average size of 2.60 μm exhibited a severe and inhomogeneous deformation. Also, SFD treatment resulted in the destroying of W skeleton due to applied load and the fracture mode changed from predominately inter-granular mode to trans-granular one. Significant reduction in tungsten particle size was also observed.

(2) Dislocation and boundaries clearly existed in the deformed W particles, and dislocation tangles were also formed. The lattice value of lattice spacing was measured to be 0.356 nm.

(3) The yield strength and ultimate tensile strength of SFDed W80-Cu20 composites were 308.74 MPa and 553.60 MPa, respectively, which were higher than those for untreated composites. The higher tensile strength of SFDed composite may be attributed to the fine W particles and high density of composites as well as the reduction of the superficial Cu phase, in particularly, the reduced grain size should be the most important factor in the increase in the tensile strength.

(4) The electrical conductivity of the sample decreased from 33 IACS% to 28.5 IACS% after SFD treatment owing to the lower Cu content in SFDed composites. Based on EDS analysis results of the wear debris, Cu content in treated composites was lower than that of untreated material due to the squeezing of Cu during the deformation process.

(5) The SFD treatment resulted in the development of a gradient microstructure due to depth of the affected material by sliding load. In other word, the content of copper phase in the near-surface areas was reduced due to squeezing of Cu during deformation, and it gradually increased with an increase in the distance from the surface of SFDed sample, and it ultimately reached the composition of the original material.

Acknowledgments

This work was supported by the National Security Major Basic Research Plan of China and the funded by Northwest Institute for Nonferrous Metal Research (K1652-11), and Newton Mobility Grant (IE161019) through Royal Society and NFSC, as well as Royal academy of Engineering UK-Research Exchange with China and India.

References

[1] L.L. Dong, M. Ahangarkani, W.G. Chen, Y.S. Zhang, Recent progress in development of tungsten-copper composites: fabrication, modification and applications, Int. J. Refract. Met. Hard

Mater. 75 (2018) 30-42.

[2] L.L. Dong, W.G. Chen, N. Deng, C.H. Zheng, Investigation on arc erosion behaviors and mechanism of W70Cu30 electrical contact materials adding graphene, J. Alloys Compd. 696 (2017) 923-930.

[3] L.L. Dong, W.G. Chen, C.H. Zheng, N. Deng, Microstructure and properties characterization of tungsten-copper composite materials doped with graphene, J. Alloys Compd. 695 (2017) 1637-1646.

[4] W.M. Daoush, J. Yao, M. Shamma, K. Morsi, Ultra-rapid processing of high-hardness tungsten-copper nanocomposites, Scr. Mater. 113 (2016) 246-249.

[5] M. Hashempour, H. Razavizadeh, H. Rezaie, Investigation on wear mechanism of thermochemically fabricated W–Cu composites, Wear, 269 (5-6) (2010) 405-415.

[6] Q. Zhou, P.W. Chen, Fabrication of W-Cu composite by shock consolidation of Cu-coated W powders, J. Alloys Compd. 657 (2016) 215-223

[7] S. Borji , M. Ahangarkani, K. Zangeneh-Madar, Z. Valefi, The effect of sintering activator on the erosion behavior of infiltrated W-10wt%Cu composite, Int. J. Refract. Met. Hard Mater. 66 (2017) 150-157.

[8] J.W. Li, F. Fang, Z. Wang, G.S. Zhang, S.Z. Wei, L.J. Xu, K.M. Pan, Microstructure and properties characterization of W-25Cu composite materials liquid-liquid doped with La_2O_3, Int. J. Refract. Met. Hard Mater.71 (2018) 115-121

[9] L. Xu, C. Srinivasakannan, L.B. Zhang, M. Yan, J.H. Peng, H.Y. Xi, S.H. Guo, Fabrication of tungsten-copper alloys by microwave hot pressing sintering, J. Alloys Compd. 658 (2016) 23-28.

[10] O. Ozer, J.-M. Missiaen, S. Lay, R. Mitteau, Processing of tungsten/copper materials from

W–CuO powder mixtures, Mat. Sci. Eng. A 460–461 (2007) 525–531

[11] Y.S. Zhang, L.C. Zhang, H.Z. Niu, X.F. Bai, S. Yu, X.Q. Ma, Z.T. Yu, Deformation twinning and localized amorphization in nanocrystalline tantalum induced by sliding friction, Mat. Lett. 127 (2014) 4–7.

[11] K. Lu, J. Lu. Nanostructured surface layer on metallic materials induced by surface mechanical attrition treatment, Mat. Sci. Eng. A 375-377 (2004) 38-45.

[12] S. Dasa, A.T. Morales, A.T. Alpasa, Microstructural evolution during high temperature sliding wear of Mg-3% Al-1% Zn (AZ31) alloy, Wear 268 (2009) 94-103.

[13] M. Wen, G. Liu, J.F. Gu, W.M. Guan, J. Lu, Dislocation evolution in titanium during surface severe plastic deformation, Appl. Surf. Sci. 255(2009) 6097–6102.

[14] Y.S. Zhang, P.X. Zhang, H.Z. Niu, C. Chen, G. Wang, D.H. Xiao, X.H. Chen, Z.T. Yu, S.B. Yuan, X.F. Bai, Surface nanocrystallization of Cu and Ta by sliding friction, Mat. Sci. Eng. A 607 (2014) 351–355.

[15] Y.S. Zhang, Q.M. Wei, H.Z. Niu, Y.S. Li, C. Chen, Z.T. Yu, X.F. Bai, P.X. Zhang, Formation of nanocrystalline structure in tantalum by sliding friction treatment, Int. J. Refrac. Met. Hard Mater. 45 (2014) 71–75.

[16] Q. Wei, T. Jiao, S.N. Mathaudhu, E. Ma, K.T. Hartwig, K.T. Ramesh, Microstructure and mechanical properties of tantalum after equal channel angular extrusion (ECAE), Mat. Sci. Eng. A 358 (2003) 266–72.

[17] Y.S. Zhang, H.Z. Niu, L.C. Zhang, X.F. Bai, X.M. Zhang, P.X. Zhang, Grain coarsening behavior in a nanocrystalline copper subjected to sliding friction, Mat. Lett. 123 (2014) 261–264.

[18] S.Q. Deng, A.Godfrey, W.Liu, C.L. Zhang, Microstructural evolution of pure copper

subjected to friction sliding deformation at room temperature, Mat. Sci. Eng. A 639 (2015) 448–455.

[19] I. Sabirov, R. Pippan, Formation of a W‐25%Cu nanocomposite during high pressure torsion, Scr. Mater. 52 (2005) 1293-1298.

[20] W.G. Chen, L.L. Dong, H. Zhang, N. Deng, Microstructure characterization of W-Cu alloy sheet produced by high temperature and high pressure, Mat. Lett. 205 (2017) 198-201.

[21] W.G. Chen, P. Feng, L.L. Dong, B. Liu, S.X. Ren, Y.Q. Fu, Experimental and theoretical analysis of microstructural evolution and deformation behaviors of CuW composites during equal channel angular pressing, Mater. Des. 142 (2018) 166–176.

[22] W.T. Huo, W. Zhang, J.W. Lu, Y.S. Zhang, Simultaneously enhanced strength and corrosion resistance of Mg-3Al-1Zn ally sheets with nano-grained surface layer produced by sliding friction treatment, J. Alloy. Compd. 720 (2017) 324-331.

[23] S.Q. Deng, A. Godfrey, W. Liu, N. Hansen, A gradient nanostructure generated in pure copper by platen friction sliding deformation, Scr. Mater. 117 (2016) 41-45.

[24] C.G. Figueroa, R. Schouwenaars, J.C. Pérez, R. Petrov, L. Kestens, Ultrafine gradient microstructure induced by severe plastic deformation under sliding contact conditions in copper, Mater. Charact. 138 (2018) 263-273.

[23] A. Singh, N.R. Tao, M. Dao, S. Suresha, Repeated frictional sliding properties of copper containing nanoscale twin, Scr. Mater. 66 (2012) 849-853.

[24] X. Gong, J.L. Fan, F. Ding, M. Song, B.Y. Huang, J.M. Tian, Microstructure and highly enhanced mechanical properties of fine-grained tungsten heavy alloy after one-pass rapid hot extrusion, Mat. Sci. Eng. A 528 (2011) 3646-3652.

[25] H. Abbaszadeh, A. Masoudi, H. Safabinesh, M. Takestani, Investigation on the characteristics of micro- and nano-structured W-15 wt.%Cu composites prepared by powder metallurgy route, Int. J. Refract. Met. Hard Mater. 30 (2012) 145 – 151.

[26] M. Amirjan, N. Parvin, K. Zangeneh-Madar, Mutual dependency of mechanical properties and contiguity in W–Cu composite, Mater. Sci. Eng. A 527 (2010) 6922–6929.

[27] X.L. Yang, J.T. Zou, S.H. Liang, P. Xiao, Z.K. Fan, Effect of Alloying Interlayer on Interfacial Bond Strength of CuW/CuCr Integral Materials, Mat. Sci. Eng. A 527 (2010) 5631-5636.

Figure captions

Fig. 1 (a) Photo showing the sample dimensions; (b) SEM image of cross-section of polished W80-Cu20 composites.

Fig. 2 (a) The designed set-up for SFT process; (b) ~ (e) an illustration of the step-by-step SFD processes [22].

Fig. 3 Observing location of the texture testing.

Fig. 4 The cross-section SEM images of (a) W80-Cu20 composites and (b) SFDed composites after 20 cycle sliding treatment, (c) and (d) statistical distribution of the W grain size of W particles in Fig. (a) and (b), respectively, (e) and (f) elemental mapping analysis results from W80-Cu20 composites and SFTed composites after 20 cycle sliding treatment, respectively.

Fig. 5. The longitudinal cross-sectioned SEM images of W80-Cu20 composites: (a) original W80Cu20 composites; (b) SFDed composite after 20 cycles; (c) in the edge area; (d) in the center area. (e) and (f) elemental mapping analysis results from W80-Cu20 composites and SFDed composites after 20 cycle sliding treatments, respectively.

Fig. 6 XRD patterns of the W80-Cu20 composites; (a) original composites and (b) SFDed composites after 20 cycle treatments.

Fig. 7 Pole figure (110), (200) and (211) of orgional W80-Cu20 composites (a) and SFDed W80-Cu20 composites (b) taken along cross section direction of the samples.

Fig. 8 (a) TEM image of W80-Cu20 composites, (b) electron diffraction pattern of position 1 in Fig. 8(a); (c) electron diffraction pattern of position 2 in Fig. 8(a); (d) TEM image of deformed W80-Cu20 composites; (e) high magnification of marked 3 zone in Fig. 8(e) and inset shows high-magnification images of twinning, (f) EDS of marked position 3 zone in Fig. 8(e).

Fig. 9 (a) Tensile stress-strain curves and (b) summaries of the data of the W80-Cu20 composites and 20 cycles SFDed composites, respectively.

Fig. 10 SEM images near the surface area of the composites (a) the original W80-Cu20 composites, (b) center area of the SFDed composites; and (c) edge area of the SFDed composite.

Fig. 11 Schematic illustrations of the deformation process of the W80-Cu20 composites during SFD process: (a) the original microstructure of the W80-Cu20 composites; (b) the collapse of the W skeleton; and (c) further deformation of the W particles.

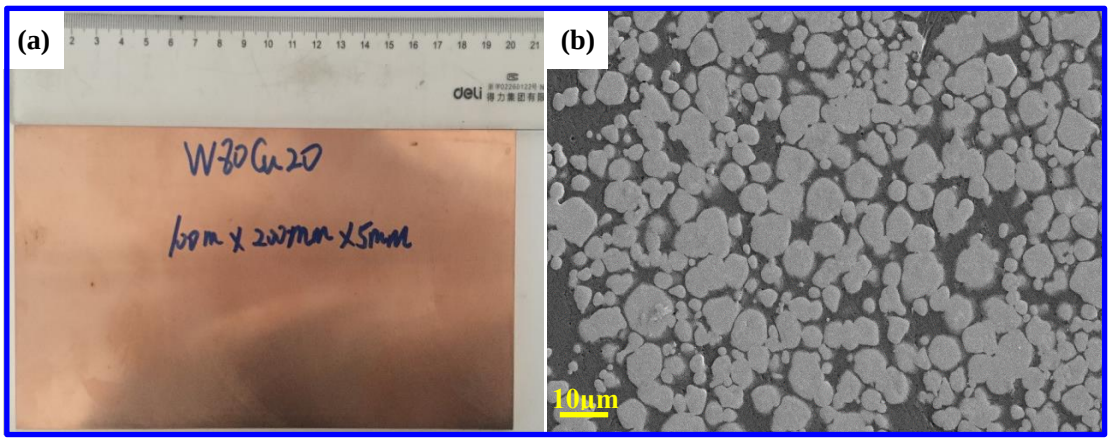

Fig. 1 (a) Photo showing the sample dimensions; (b) SEM image of cross-section of polished W80-Cu20 composites.

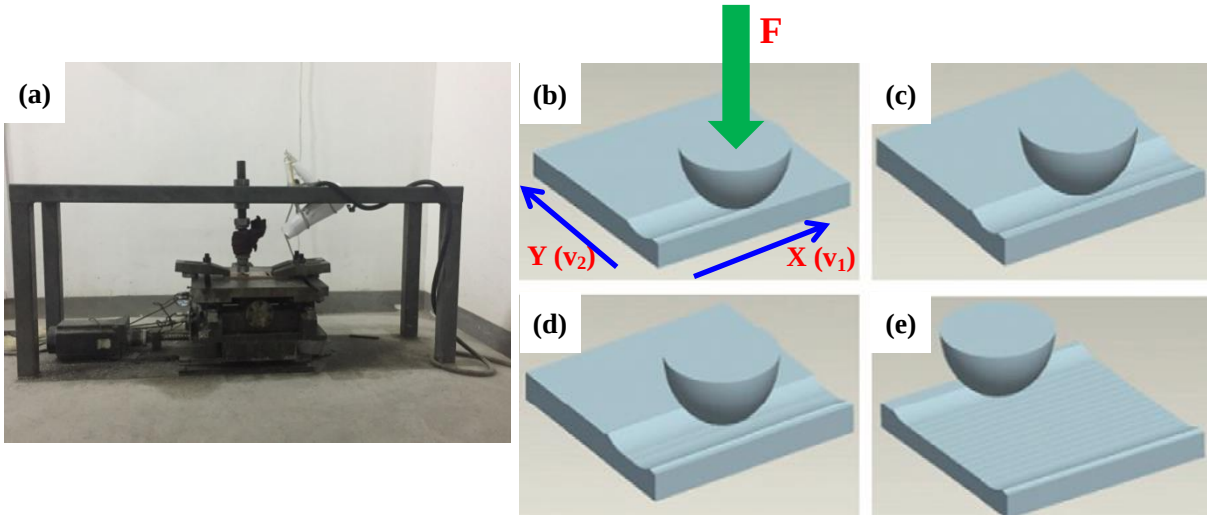

Fig. 2 (a) The designed set-up for SFD process; (b) ~ (e) an illustration of the step-by-step SFD processes [22].

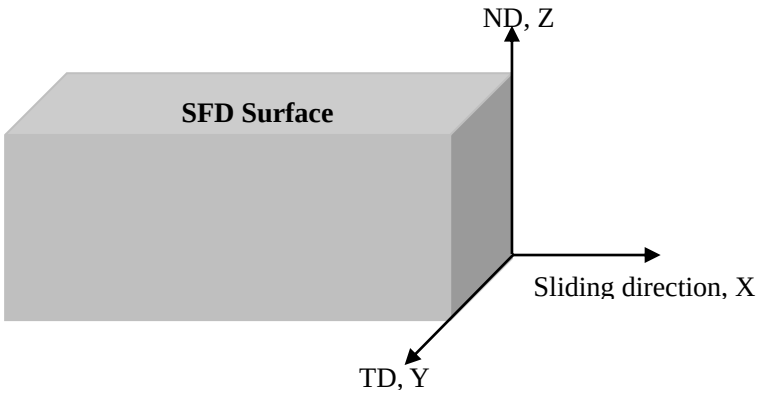

Fig. 3 Observing location of the texture testing.

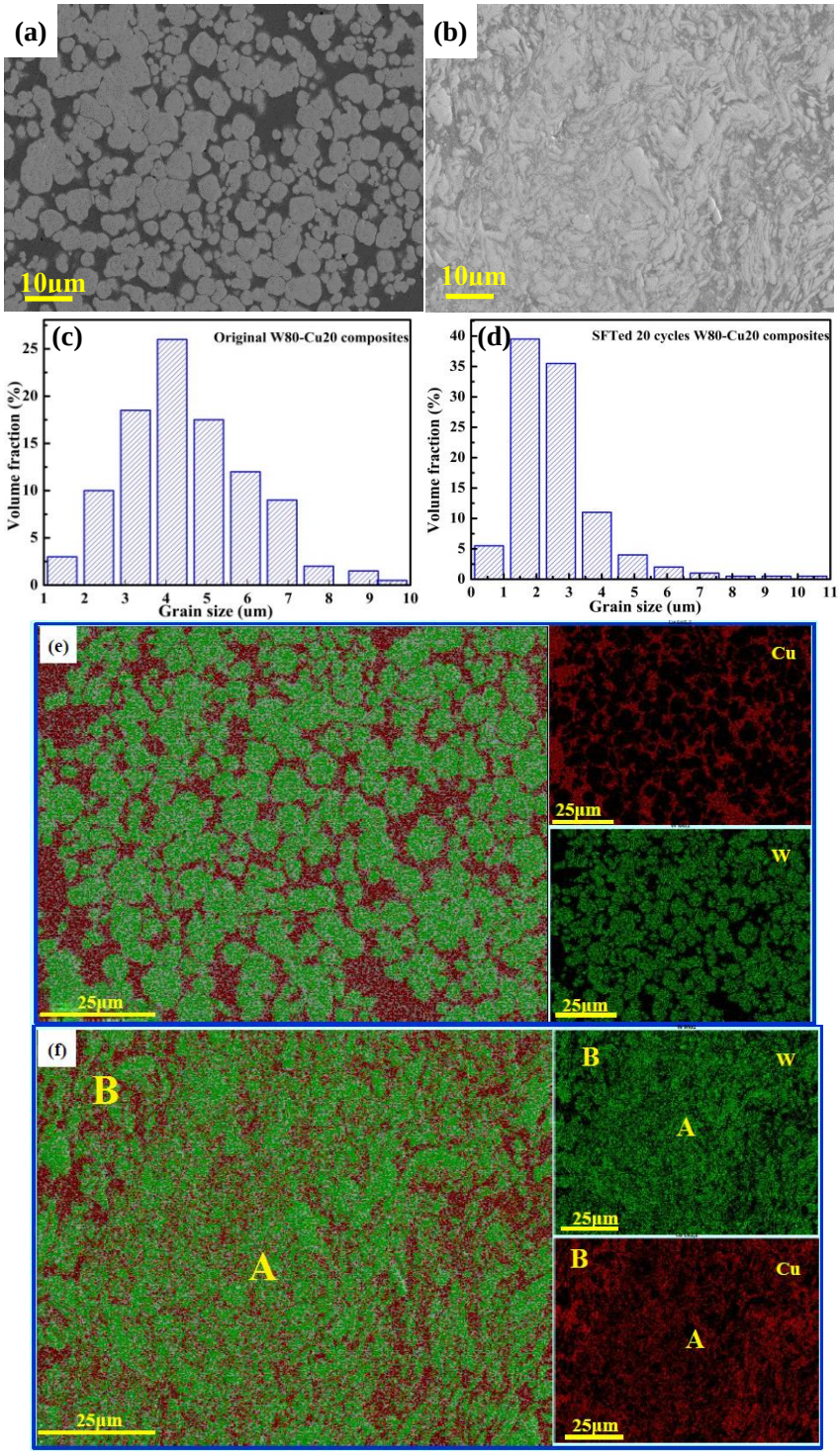

Fig. 4 The cross-section SEM images of (a) W80-Cu20 composites and (b) SFDed composites after 20 cycle sliding treatment, (c) and (d) statistical distribution of the W grain size of W particles in Fig. (a) and (b), respectively, (e) and (f) elemental mapping analysis results from W80-Cu20 composites and SFDed composites after 20 cycle sliding treatment, respectively.

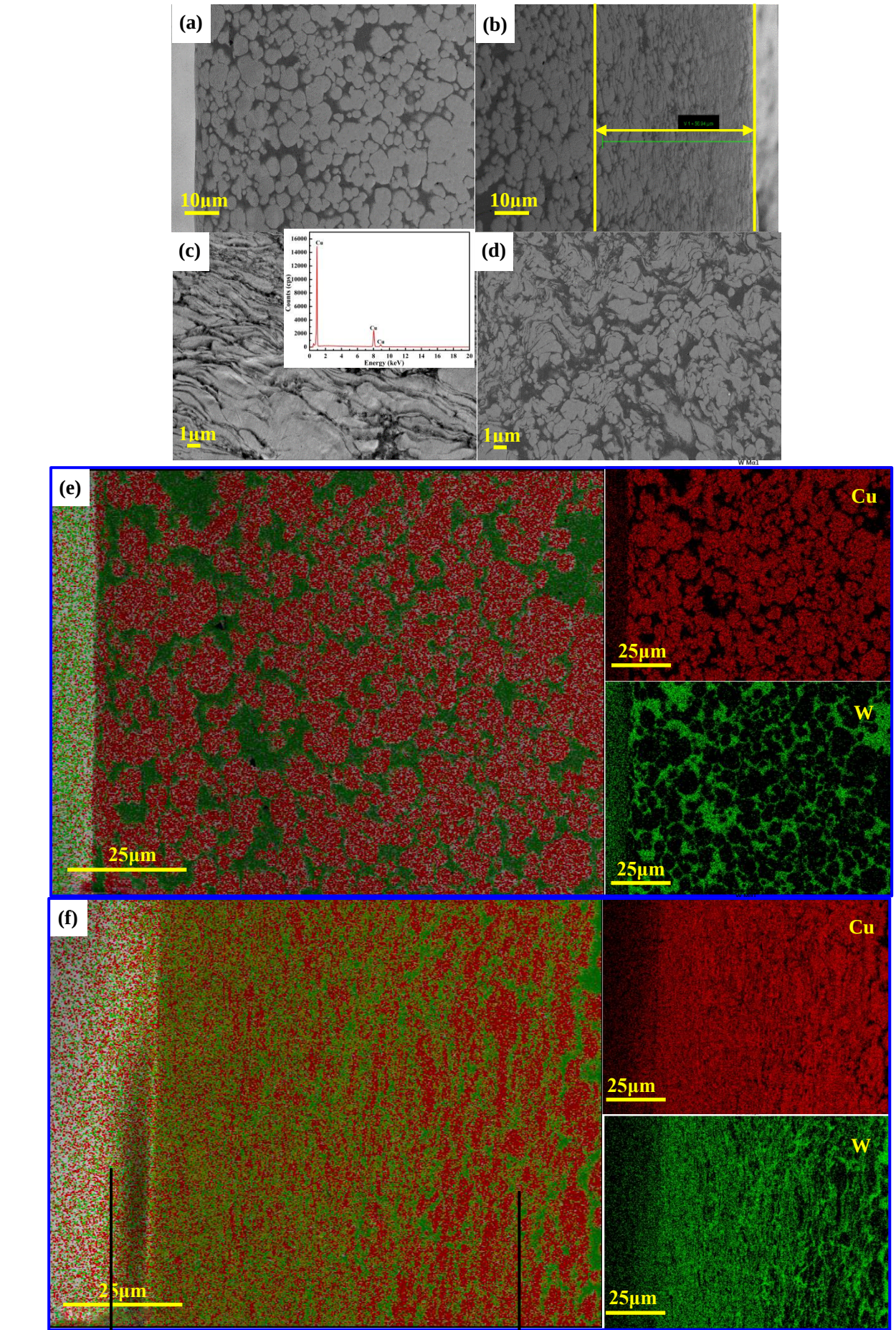
(a)
10μm
(b)
10μm
(c)
Cu
Cu
Energy (keV)
1μm
(d)
1μm
(e)
25μm
Cu
25μm
W
25μm
(f)
25μm
Cu
25μm
W
25μm
Region containing lower Cu phase content
Region containing higher Cu phase content
Gradually change in Cu content

Fig. 5. The longitudinal cross-sectioned SEM images of W80-Cu20 composites: (a) original W80Cu20 composites; (b) SFDed composite after 20 cycles; (c) in the edge area; (d) in the center area. (e) and (f) elemental mapping analysis results from W80-Cu20 composites and SFDed composites after 20 cycle sliding treatments, respectively.

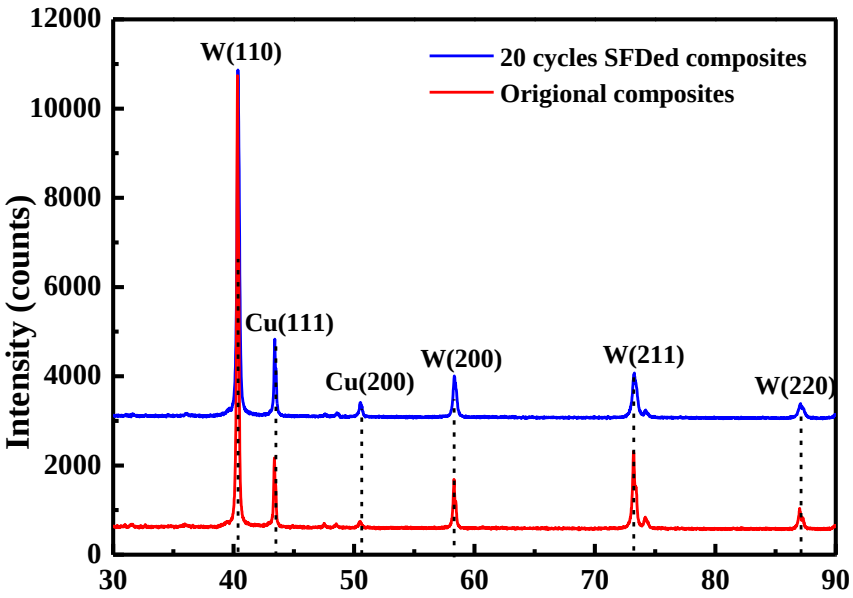

Fig. 6 XRD patterns of the W80-Cu20 composites; (a) original composites and (b) SFDed composites after 20 cycle treatments.

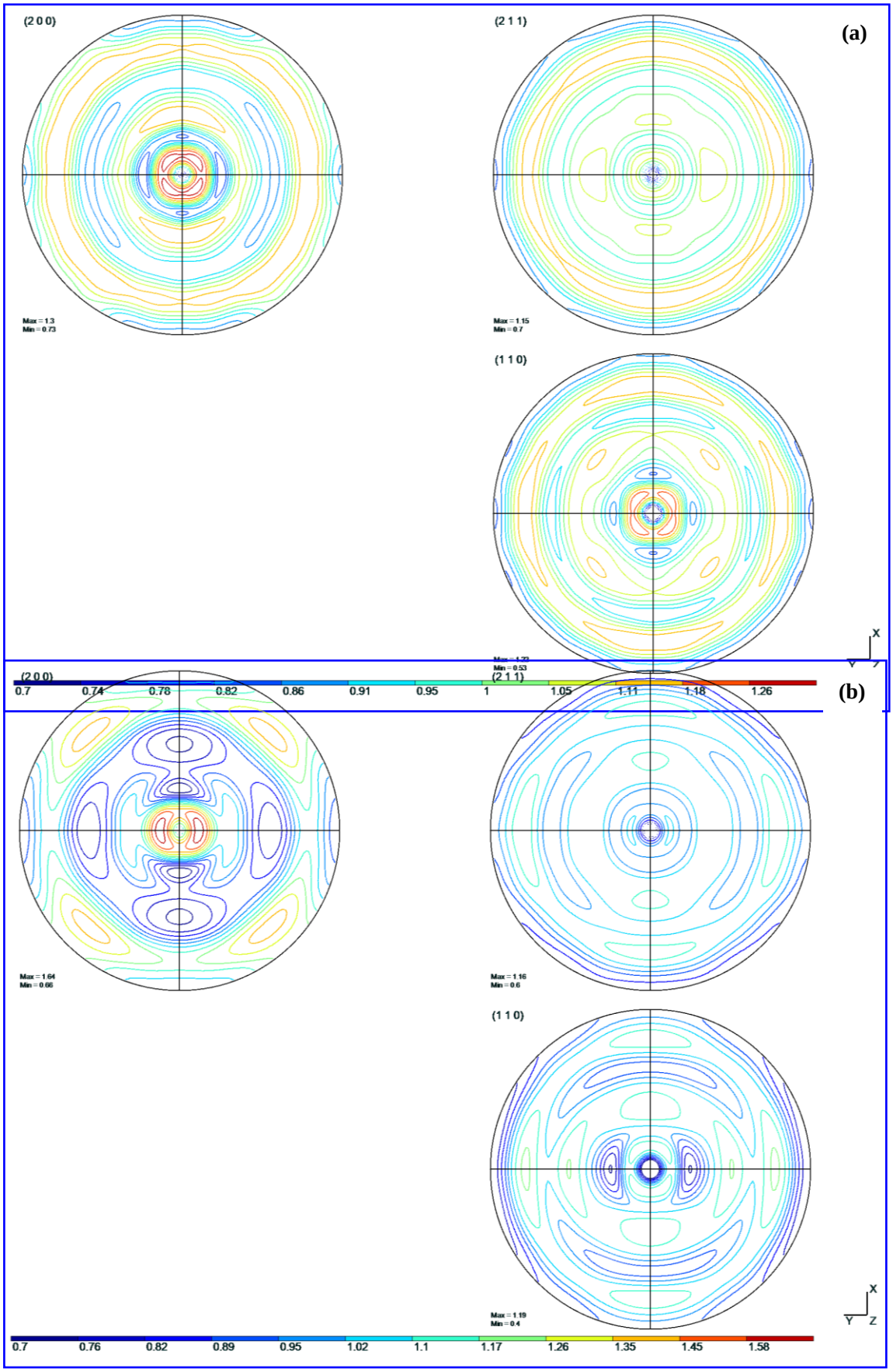
(a)
(2 0 0)
Max = 1.3
Min = 0.73
(2 1 1)
Max = 1.15
Min = 0.7
(1 1 0)
Max = 1.23
Min = 0.53
X
Y
Z
(b)
(2 0 0)
0.7 0.74 0.78 0.82 0.86 0.91 0.95 1 1.05 1.11 1.18 1.26
Max = 1.64
Min = 0.66
(2 1 1)
Max = 1.16
Min = 0.6
(1 1 0)
Max = 1.19
Min = 0.4
0.7 0.76 0.82 0.89 0.95 1.02 1.1 1.17 1.26 1.35 1.45 1.58
X
Y
Z

Fig. 7 Pole figure (110), (200) and (211) of orgional W80-Cu20 composites (a) and SFDed W80-Cu20 composites (b) taken along cross section direction of the samples.

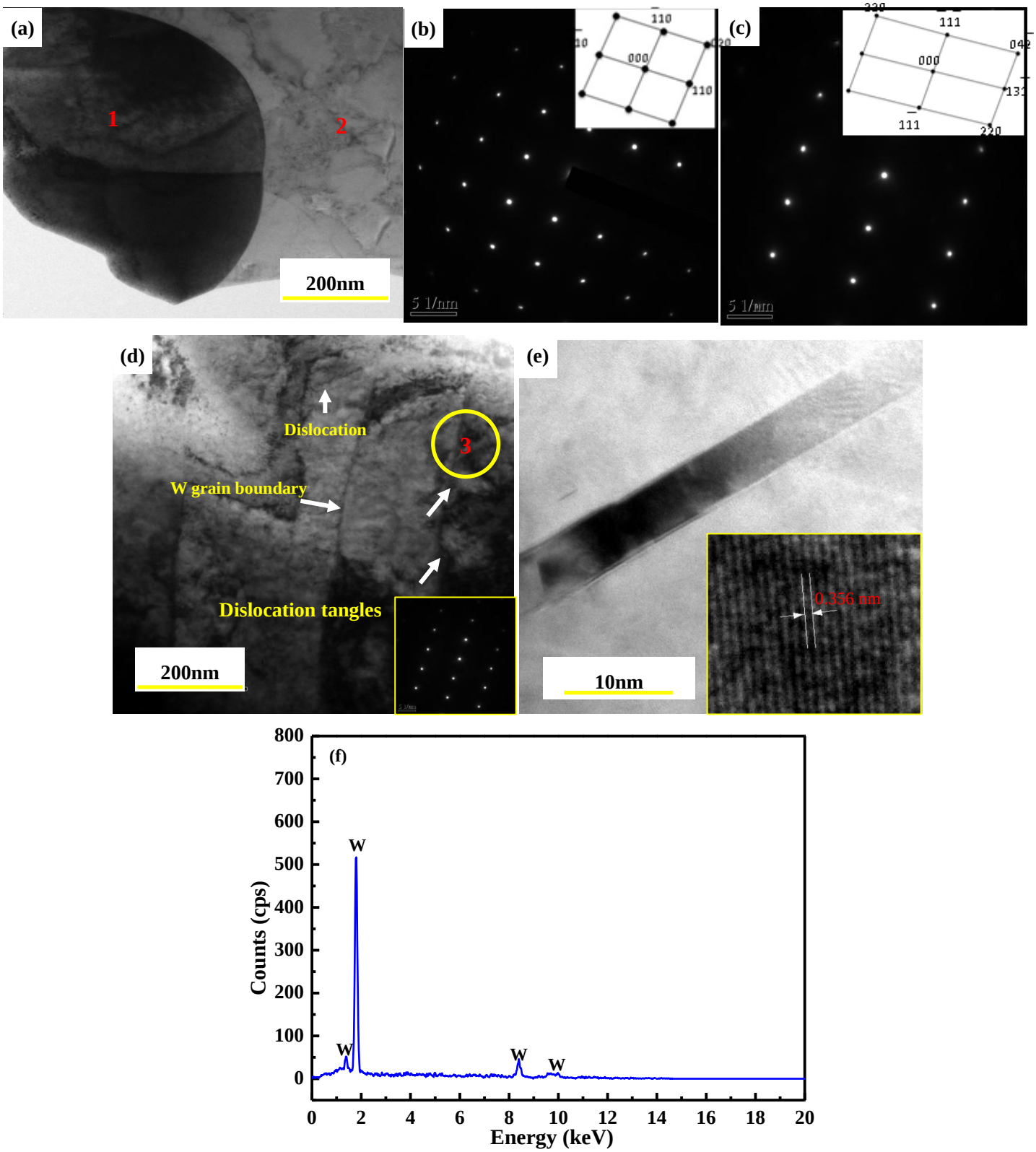

Fig. 8 (a) TEM image of W80-Cu20 composites, (b) electron diffraction pattern of position 1 in

Fig. 8(a); (c) electron diffraction pattern of position 2 in Fig. 8(a); (d) TEM image of deformed W80-Cu20 composites; (e) high magnification of marked 3 zone in Fig. 8(e) and inset shows high-magnification images of twinning, (f) EDS of marked position 3 zone in Fig. 8 (e).

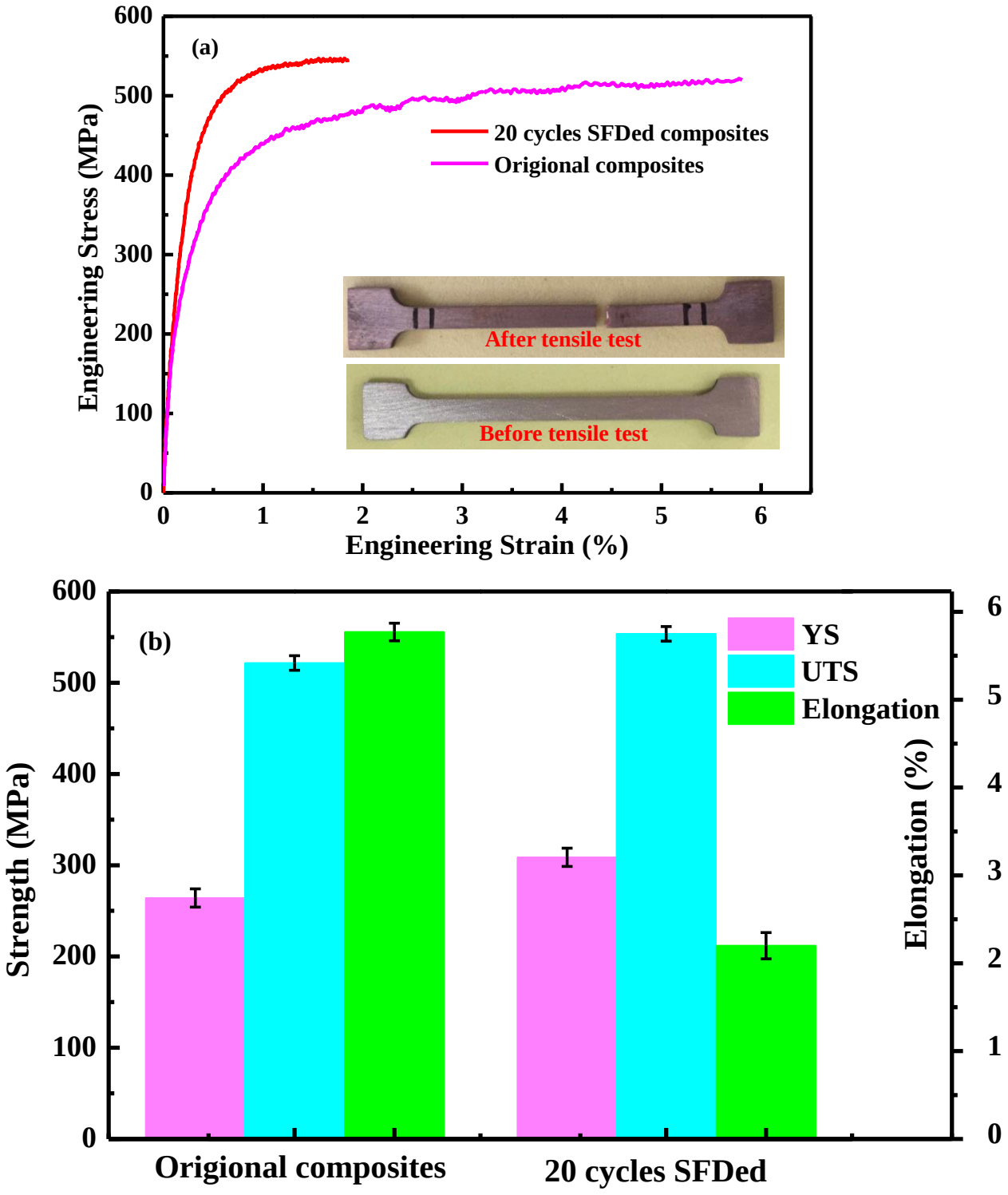

Fig. 9 (a) Tensile stress-strain curves and (b) summaries of the data of the W80-Cu20 composites

and 20 cycles SFDed composites, respectively.

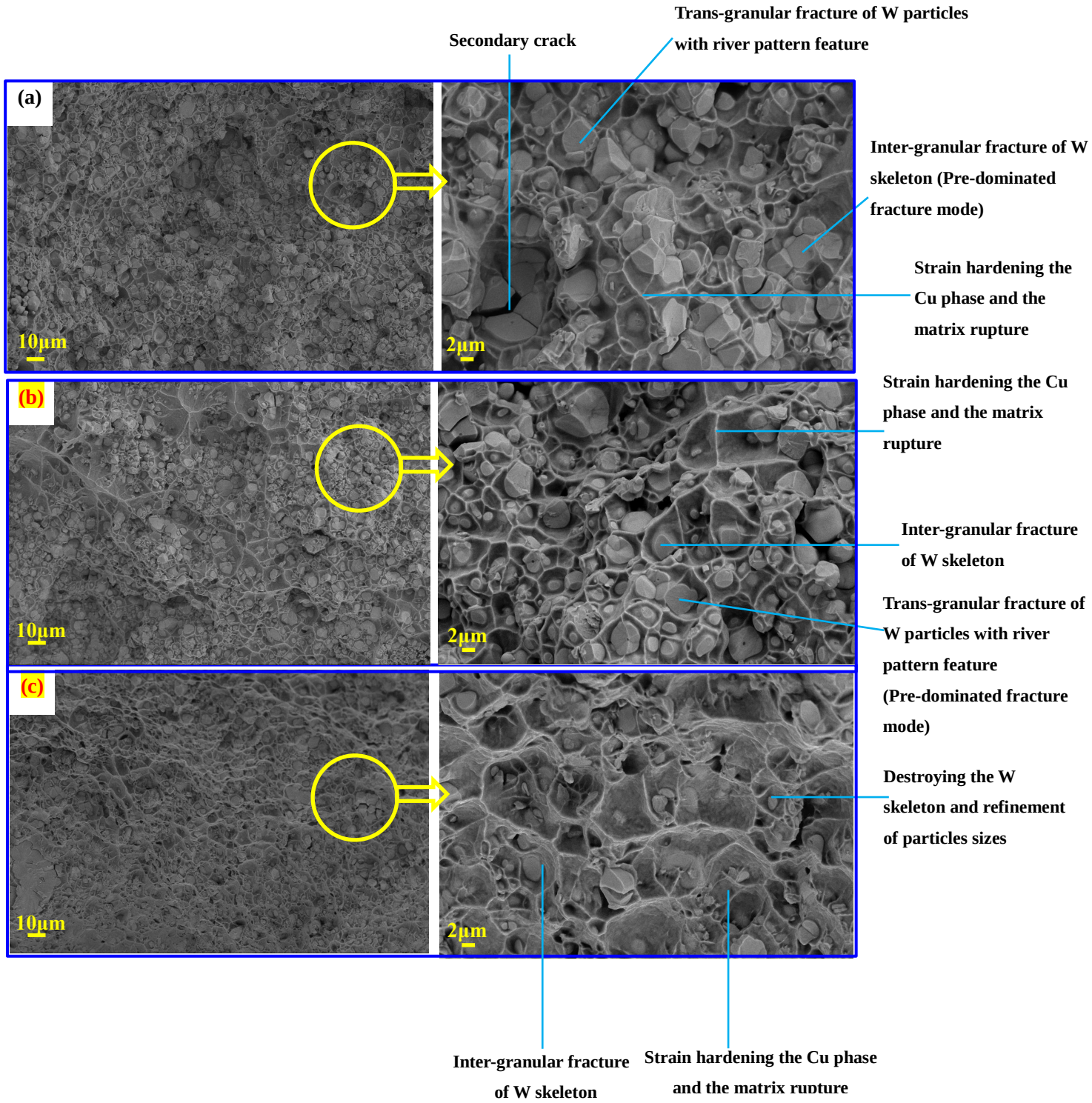

Fig. 10 SEM images near the surface area of the composites (a) the original W80-Cu20 composites, (b) center area of the SFDed composites; and (c) edge area of the SFDed composite.

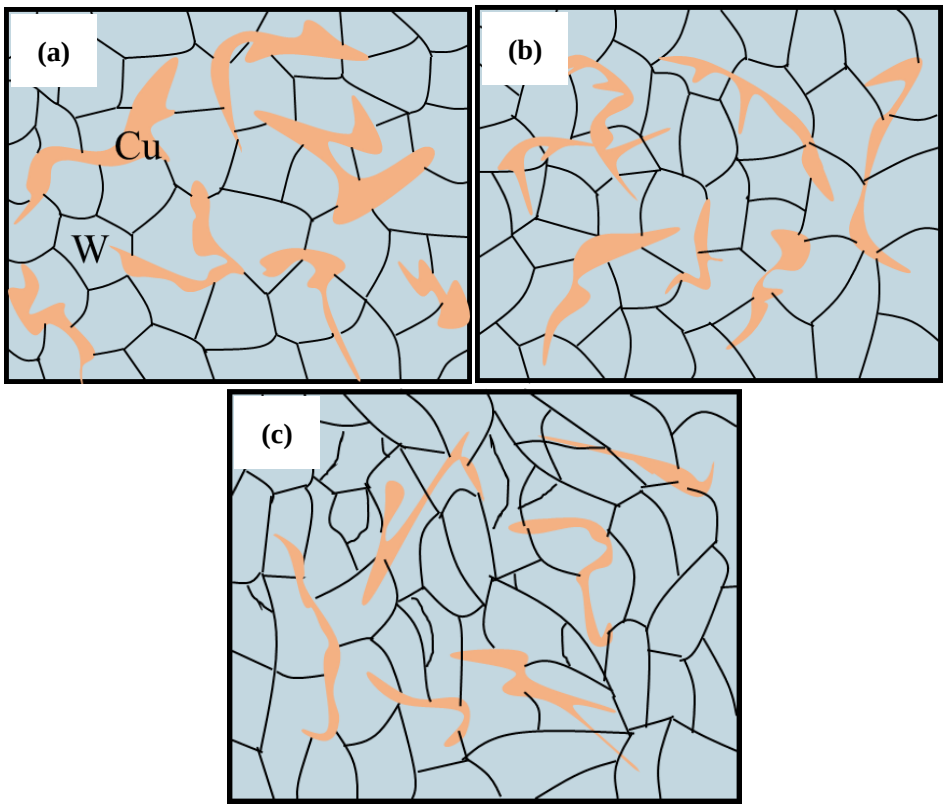

Fig. 11 Schematic illustrations of the deformation process of the W80-Cu20 composites during SFD process: (a) the original microstructure of the W80-Cu20 composites; (b) the collapse of the W skeleton; and (c) further deformation of the W particles, respectively.

Tables captions

Table 1. Processing parameters of fabrication of W80-Cu20 composites by hot pressing sintering.

Table 2 The electrical conductivity, relative density and micro-hardness of the W80-Cu20 composites in the work.

Table 1. Processing parameters of fabrication of W80-Cu20 composites by hot pressing sintering.

Sample	Processing parameters	Values
W80-Cu20 composites	Temperature (^{o}C)	1500
	Holding time (min)	120
	Pressure (MPa)	30

Table 2 The electrical conductivity, relative density and micro-hardness of the W80-Cu20 composites in the work.

	Original	SFDed
Electrical conductivity/ IACS%	33	30.5
Relative density/ %	96	98.5
Micro-hardness/ HV	214.5	308

* Electrical conductivity reported as percentage of international annealed copper standard (%IACS).